Journal of Rare Earths 39 (2021) 487–494

Contents lists available at ScienceDirect

Journal of Rare Earths

journal homepage: http://www.journals.elsevier.com/journal-of-rare-earths

Metal–organic frameworks of lanthanide iminodiacetates and tartrates: Synthesis, structural characterization and luminescence properties — Commemorating the 100th anniversary of the birth of Academician Guangxian Xu☆

Melissa Fairley [a, †], M.M. Varuni S. Livera [a, †], Wanmin Chen [b], Jorge H.S.K. Monteiro [c], Adam Schmitt [a], Ana de Bettencourt-Dias [c, **], Sue Roberts [a], Zhiping Zheng [a, b, *]

[a] Department of Chemistry and Biochemistry, University of Arizona, Tucson, AZ 85721, USA
[b] Department of Chemistry, Southern University of Science and Technology, Shenzhen 518055, China
[c] Department of Chemistry, University of Nevada, Reno, NV 89557, USA

ARTICLE INFO

Article history:
Received 3 November 2020
Received in revised form
14 January 2021
Accepted 27 January 2021
Available online 5 February 2021

Keywords:
Lanthanides
Metal–organic frameworks
Luminescence
Rare earths

ABSTRACT

Two series of lanthanide-containing metal–organic frameworks (Ln-MOFs) of the general formula $\{[Ln(HIDA)_2H_2O]ClO_4 \cdot H_2O\}_n$ (Ln = La (**1**), Nd (**2**), Eu (**3**), Gd (**4**), Tb (**5**), Eu:Tb (**6**); H_2IDA = iminodiacetic acid) and $[Ln(TT)(HTT)(H_2O)_3]_n$ (Ln = Eu (**7**), Gd (**8**), Tb (**9**), Dy (**10**), and Eu:Tb (**11**); H_2TT = tartaric acid) were synthesized by reacting $Ln(ClO_4)_3$ with iminodiacetic acid and *L*-tartaric acid, respectively. All compounds were structurally characterized by single-crystal X-ray diffraction. Elemental analyses are consistent with the corresponding crystallographically generated formulas. Moreover, the luminescence properties of both the single and mixed-lanthanide complexes were studied. Near infrared, red, and green emissions that are characteristic of Nd(III), Eu(III), and Tb(III) are observed for **2**, **3**/**7**, and **5**/**9**, respectively. For the two mixed-lanthanide complex systems **6** and **11**, depending on the relative amount of Eu(III) and Tb(III), the color of emission can be fine-tuned. It is found that a small amount of Eu(III) is adequate for the observation of the most intense transition of Eu(III). This is believed to be a result of energy transfer from Tb(III) to Eu(III) within the same complex - a conclusion supported by the significantly shortened lifetime of Tb(III) and the accompanying enhanced lifetime of Eu(III) in the mixed-lanthanide complex with respect to the corresponding values for the pure Tb(III) and Eu(III) complexes with the same ligand.

1. Introduction

Lanthanide-containing metal–organic frameworks (Ln-MOFs) are a relatively new class of materials with potential applications for sensing[1–10] and white-light production.[11–16] While sensory systems sensitively and selectively recognize specific analytes of biological and environmental significance,[1,2,5,8–10,16–19] materials capable of light-emission at various wavelengths and color-tuning are important for solid-state lighting, large-panel displays, telecommunication, and biomedical imaging.[7,15,20–23] These applications are made possible primarily because of the unique f-electronic structure of the lanthanide ions. Specifically, upon appropriate excitation, light-emissions in the wide range between near infrared and ultraviolet can be generated, with Eu(III) and Tb(III) emitting respectively in red and green being the most extensively studied.[7,24,25] Due largely to the similar lanthanide sizes, the chemical reactivity of the lanthanide ions is comparable, so much so that isostructural complexes are frequently obtained with the use of different lanthanide ions under otherwise the same reaction conditions.[26,27] This offers the possibility of color tuning of light emission, as a product incorporating different lanthanide ions

☆ **Foundation items:** Project partially supported by US NSF grant CHE-1800392 (AdBD).

* Corresponding author. Department of Chemistry and Biochemistry, University of Arizona, Tucson, AZ 85721, USA.
** Corresponding author.
E-mail addresses: abd@unr.edu (A. de Bettencourt-Dias), zhengzp@sustech.edu.cn (Z. Zheng).
† These two authors contributed equally to this work.

https://doi.org/10.1016/j.jre.2021.01.019
1002-0721/

can be produced with the use of a lanthanide mixture.[9,11,15–17] One can anticipate photophysical properties that are different from those observed for single-lanthanide complexes, as energy transfer between different lanthanide centers within the same complex may occur.[10,11,21–23,28]

A large number of Ln-MOFs have been reported, most of which feature di- or polycarboxylate-based bridging ligands due to the strong oxophilicity of the lanthanide ions.[8,14,17,20,23,29–37] Often such work is concerned with only the synthesis and structural determination of the framework structures of the single-lanthanide complexes. In this work, we report two series of Ln-MOFs using two commonly available carboxylic acids, namely iminodiacetic acid (H_2IDA) and *L*-tartaric acid (H_2TT) as the organic linkers (Fig. 1). All complexes, either new or previously reported, were structurally characterized by single-crystal X-ray diffraction. Photophysical properties of these complexes with Ln = Nd(III), Eu(III), Gd(III), and Tb(III) were studied. We also prepared a number of mixed-lanthanide complexes with different molar ratios of Eu/Tb, with which tuning of the color of emissions was visually observed. Detailed luminescence studies revealed interesting intramolecular energy transfer from Tb(III) to Eu(III).

2. Materials and methods

2.1. Materials and characterization

Lanthanide oxides and other reagents were purchased and used without further purification. Aqueous solutions of $Ln(ClO_4)_3$ (Ln = Eu, Tb, Nd, La, Gd) were prepared by dissolving the corresponding lanthanide oxides in concentrated $HClO_4$ and then diluting to 1.0 mol/L. Elemental analyses (CHN) were performed on a PerkinElmer PE2400-Series II, CHNS/O analyzer. Elemental analysis for Eu and Tb in complex **6** was obtained using an Elan DRC-II inductively coupled plasma-mass spectrometer (ICP-MS) system. Elemental analyses of Eu and Tb in complexes **11a**–**e** were obtained by using an iCAP 7400 ICP-OES Thermo Scientific system. The molar ratios of the starting Tb(III)/Eu(III) and those in the products determined by ICP analysis are shown in Table S1 (Supporting Information).

2.2. X-ray crystallographic studies

Single crystal X-ray diffraction data were collected on a Bruker APEX II Duo X-ray diffractometer with graphite-monochromated Mo Kα radiation (λ = 0.071073 nm) at room temperature. The structures were solved by direct methods and refined by full-matrix least squares using SHELXTL[38] in Olex2. SAINT software was used to integrate the data and multi-scan absorption corrections were applied using SADABS[39] and absorption corrections were applied using TWINABS.[39] All non-hydrogen atoms were refined with anisotropic thermal parameters. Hydrogen atoms were located at geometrically calculated positions and refined with isotropic thermal parameters. The relevant crystal data and details of the data collection and refinement are summarized in Tables S2 and S3. More details on the crystallographic studies and atomic displacement parameters can be found in the CIF files (Supporting Information). Powder X-ray diffraction studies were performed in the $2\theta = 7°–50°$ range on a Philips X'Pert MPD with Cu Kα (λ = 0.1542 nm) at room temperature.

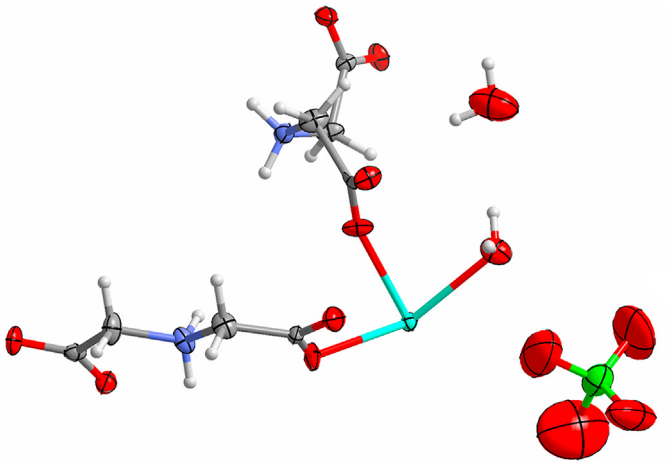

Fig. 1. The asymmetric unit of the crystal structure of **3**. Color legend: Eu (cyan), O (red), C (grey), N (purple), Cl (green), and H (white).

2.3. Photoluminescence studies

The photoluminescence data for **3**, **5**, and **6** were obtained by a Fluorolog-3 spectrofluorometer (Horiba FL3-22-iHR550), with a 1200 grooves/mm excitation monochromator with gratings blazed at 330 nm and a 1200 grooves/mm emission monochromator with gratings blazed at 500 nm. A 450 W ozone-free xenon lamp (Ushio) was used as the radiation source. The excitation spectra corrected for instrumental function were measured between 250 and 500 nm. The emission spectra were measured in the range of 450–725 nm in front face mode at 22.5°. All emission spectra were corrected for instrumental function. The emission decay curves were obtained using a TCSPC system and a Xe pulsed lamp as excitation source. The time-resolved phosphorescence spectra of the analogous Gd(III) complex were obtained at 77 K on a PerkinElmer LS-55 spectrometer. The energy of the ligand's triplet state was obtained by deconvolution of the phosphorescence spectrum into its Franck-Condon progression with the highest energy component taken as the 0-0 transition.[40] Unless otherwise indicated, all spectrophotometric measurements were carried out at room temperature. The efficiency of energy transfer between Tb(III) and Eu(III) (η_{ET}) was calculated according to Eq. (1):

$$\eta_{ET} = 1 - \frac{\tau_{TbEu}}{\tau_{Tb}} \quad (1)$$

τ_{TbEu} is the lifetime of the $^5D_4 \rightarrow {}^7F_5$ transition of the mixed-ion complex and τ_{Tb} is the lifetime of that same transition for the Tb(III) complex. Photoluminescence data for complexes **7**, **9**, and **11a**–**e** were collected at room temperature using a QuantumMaster 40 PTI fluorimeter with a 75 W Xe arc excitation lamp and a photomultiplier tube at 1100 V. A slit width of 1 nm and integration time of 2 s were used during data collection. The angle of incidence on a sample goniometer was set to 60°. Solid samples were prepared by depositing powder on carbon tape mounted to a glass slide.

2.4. Samples preparation

2.4.1 Synthesis of $\{[Ln(HIDA)_2H_2O]ClO_4 \cdot H_2O\}_n$ (Ln= La (1), Nd (2), Eu (3), Gd (4), Tb (5)).

A reaction mixture containing $Ln(ClO_4)_3$ (2 mL, 1.0 mol/L) and iminodiacetic acid (H_2IDA; 0.266 g, 2.0 mmol) in 10 mL of water was stirred at 80 °C while a freshly prepared aqueous solution of NaOH (1.0 mol/L) was added slowly to the point of incipient but permanent precipitation. The mixture was kept under reflux for 5 h and then filtered while hot. The filtrate was collected and covered with a parafilm to allow for evaporation under ambient conditions. Colorless crystals, obtained after about one week, were collected,

washed with chilled water, and dried under vacuum. Elemental analysis (%):

Calcd for $C_8H_{16}N_2O_{14}ClLa$ (**1**): C, 17.84; H, 2.99; N, 5.20. Found: C, 18.09; H, 2.86; N, 5.44.

Calcd for $C_8H_{16}N_2O_{14}ClNd$ (**2**): C, 17.67; H, 2.96; N, 5.15. Found: C, 17.73; H, 2.67; N, 5.14.

Calcd for $C_8H_{16}N_2O_{14}ClEu$ (**3**): C, 17.42; H, 2.92; N, 5.08. Found: C, 17.47; H, 2.99; N, 5.10.

Calcd for $C_8H_{16}N_2O_{14}ClGd$ (**4**): C, 17.25; H, 2.90; N, 5.03. Found: C, 17.55; H, 2.72; N, 5.22.

Calcd for $C_8H_{16}N_2O_{14}ClTb$ (**5**): C, 17.20; H, 2.89; N, 5.01. Found: C, 17.05; H, 2.65; N, 4.94.

2.4.2 Synthesis of $\{[(Eu/Tb)(HIDA)_2H_2O]ClO_4\cdot H_2O\}_n$ (6).

This compound was prepared by following a similar procedure as is described above for compounds **1**–**5**, but using a mixture of $Eu(ClO_4)_3$ (0.2 mL, 1.0 mol/L) and $Tb(ClO_4)_3$ (3 mL, 1.0 mol/L). Elemental analysis (%): Calcd for $C_8H_{14}N_2O_{16}Cl(Eu/Tb)$ (**6**): C, 17.26; H, 2.54; N, 5.03. Found: C, 17.20; H, 2.49; N, 5.07. The molar ratio of Eu:Tb was determined to be 1.0:8.3 in this mixed lanthanide complex.

2.4.3 Synthesis of $[Ln(TT)(HTT)\cdot 3H_2O]_n$ (Ln= Eu (7), Gd (8), Tb (9), Dy (10)).

L-tartaric acid (0.15 g, 1.0 mmol) was dissolved in 4 mL of $Ln(ClO_4)_3$ (aq. 1.0 mol/L) and stirred at 80 °C, to which a freshly prepared solution of NaOH (aq. 0.5 mol/L) was added to the point of incipient but permanent precipitation. The resulting mixture was then filtered while hot. The filtrate was collected and covered with parafilm for slow evaporation. Block-shaped colorless crystals formed after approximately one week. The crystals were collected by filtration, washed with chilled water, and dried under vacuum. Elemental analysis (%):

Calcd for $C_8H_{15}O_{15}Eu$ (**7**): C, 19.10; H, 3.01. Found: C, 19.28; H, 2.92.

Calcd for $C_8H_{15}O_{15}Gd$ (**8**): C, 18.90; H, 2.97. Found: C, 19.09; H, 3.15.

Calcd for $C_8H_{15}O_{15}Tb$ (**9**): C, 18.84; H, 2.96. Found: C, 18.85; H, 3.01.

Calcd for $C_8H_{15}O_{15}Dy$ (**10**): C, 18.70; H, 2.94. Found: C, 18.94; H, 2.70.

2.4.4 Synthesis of $[(Eu/Tb)(TT)(HTT)\cdot 3H_2O]_n$ (11a–e).

This series of compounds were prepared by following a similar procedure as is described for **7**–**10**, but using a mixture of $Eu(ClO_4)_3$ and $Tb(ClO_4)_3$ in the following Eu:Tb molar ratios: 7:1 (**11a**), 3:1 (**11b**), 1:1 (**11c**), 1:3 (**11d**), and 1:7 (**11e**), respectively. The products were obtained as polycrystalline solids. Elemental analysis (%):

Calcd for **11a** (Eu:Tb = 7:1): C, 19.05; H, 3.00. Found: C, 19.21; H, 2.80.

Calcd for **11b** (Eu:Tb = 3:1): C, 19.01; H, 2.99. Found: C, 19.31; H, 2.66.

Calcd for **11c** (Eu:Tb = 1:1): C, 18.95; H, 2.98. Found: C, 19.06; H, 2.74.

Calcd for **11d** (Eu:Tb = 1:3): C, 18.89; H, 2.97. Found: C, 19.13; H, 2.57.

Calcd for **11e** (Eu:Tb = 1:7): C, 18.85; H, 2.97. Found: C, 19.09; H, 2.57.

3. Results and discussion

3.1. Syntheses

The two series of compounds, namely $\{[Ln(HIDA)_2H_2O]ClO_4\cdot H_2O\}_n$ (**1**–**6**) and $[Ln(TT)(HTT)(H_2O)_3]_n$ (**7**–**11**), were prepared using similar procedures but with iminodiacetic acid (H_2IDA) and *L*-tartaric acid (H_2TT) as ligands, respectively. These include the mixed-lanthanide complexes **6** and **11a**–**e**. We note that the molar ratios of Eu/Tb in the final products are not the same as the original ones in the starting mixtures. Specifically, for the synthesis of **6**, single crystals were obtained only when a starting Eu/Tb ratio of 1.0:15 was used. However, elemental analysis by ICP-MS yielded a ratio of 1.0:8.3, suggesting that some of the starting Tb(III) was not incorporated. This argument is supported by the green luminescence, characteristic of Tb(III), upon UV irradiation of the mother liquor. Interestingly, in the case of mixed-lanthanide tartrates, the molar Eu/Tb ratios in the final products agreed well with those in the reactants; the reason for the observed disparity remains unclear.

If the nature of the lanthanide is not considered, it appears that the chemical compositions of **1**–**6** are the same, although they crystallized out in different space groups depending on the lanthanide ion used (see below for structural description); those of lighter lanthanides (**1**–**3**) crystallized out in the space of $P2_1/c$, whereas those with heavier ones (**4** and **5**) crystallized out in the space group of *P*-1. The mixed-lanthanide complex **6** also crystallized out in *P*-1, which interestingly suggests that the resulting space group is determined by the "averaged" lanthanide, that is, Gd(III) which is between the two lanthanide ions (Eu(III) and Tb(III)) used. However, all complexes (**7**–**10**) featuring tartrate as ligand crystallized out in the same space group of $P4_12_12$.

3.2. Structural description

Several extended Ln-IDA complexes have been reported,[30–34] including examples with transition metals[41–43] and mixed-ligand systems.[44,45] Examples of mixed Ln-IDA extended structures to produce white light are not known. The structure of **3** is presented in detail as a representative of the isostructural **1** and **2**; the structures are only slightly different in their unit-cell dimensions and volumes, as a result of the small difference in the size of the lanthanide ions.

The asymmetric unit consists of one Eu(III) ion, two $HIDA^-$ ligands, one aqua ligand, one ClO_4^-, and one water solvent molecule. $HIDA^-$ is a result of the protonation of the imino group of the doubly deprotonated IDA^{2-} ligand.

The Eu(III) ion is octa-coordinate featuring the coordination by eight O atoms, seven of which being from seven different $HIDA^-$ ligands and one from the aqua ligand. The coordination geometry can be best described as a distorted square antiprism. The Eu–O bond lengths, ranging from 0.23571 to 0.24965 nm with an average of 0.2414 nm, are typical of similar carboxylate Eu(III) complexes.[27,46] The $HIDA^-$ ligand, serving as a tetradentate linker, coordinates the Eu(III) ion using only its 4 carboxylate O atoms in a μ_4-κO:κO':κO'':κO''' bridging mode; such a mode has not yet been reported, although a large number of lanthanide complexes with $HIDA^-$ are known.[31–33] Crystallographic analysis reveals that the protonated imino group is hydrogen-bonded with a ClO_4^- ion present in the voids of the extended framework structure (Fig. 2).

Each Eu(III) is bridged to two Eu(III) through two bridging carboxylate groups of the IDA ligand and to nine Eu(III) through the opposite carboxylate group of the IDA linker. The framework structure features two types of channels, one having a dimension of approximately 0.723 nm × 0.504 nm (Fig. 3(a)) and the other 0.603 nm × 0.833 nm (Fig. 3(b)). This structure is similar to a previously reported $[Ln_2(H_2O)_4(HIDA)_2(IDA)]Cl_2\cdot 3H_2O$ (Ln = Pr[32], Nd[31]) with an additional $HIDA^-$ linking metal nodes in place of H_2O molecules.

Crystallographic studies of **4**–**6** showed that they are also isostructural, but in the triclinic *P*-1 space group. Nevertheless, the coordination modes are essentially the same; the difference from the structure of **3** is only the relative position of the ligands. Such disparities can be clearly seen from the structure of **3** versus that of

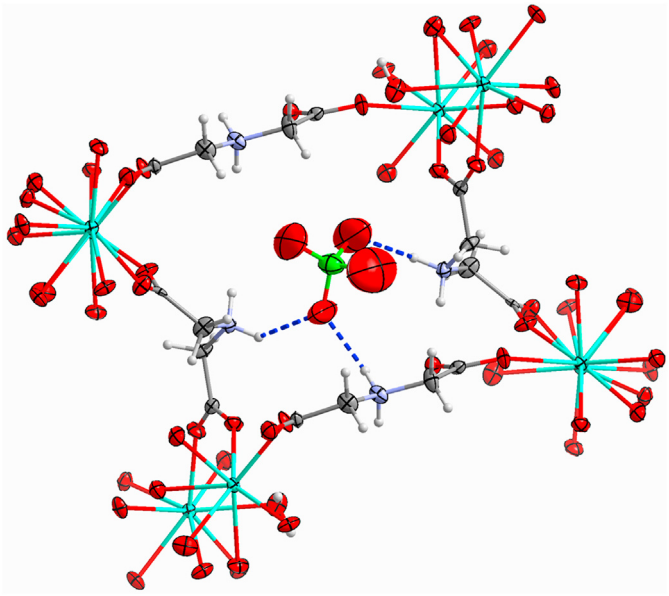

Fig. 2. H-bonding interaction of ClO_4^- ion and protonated imino group (blue dotted line). Color legend: Eu (cyan), O (red), C (grey), N (purple), Cl (green), and H (white).

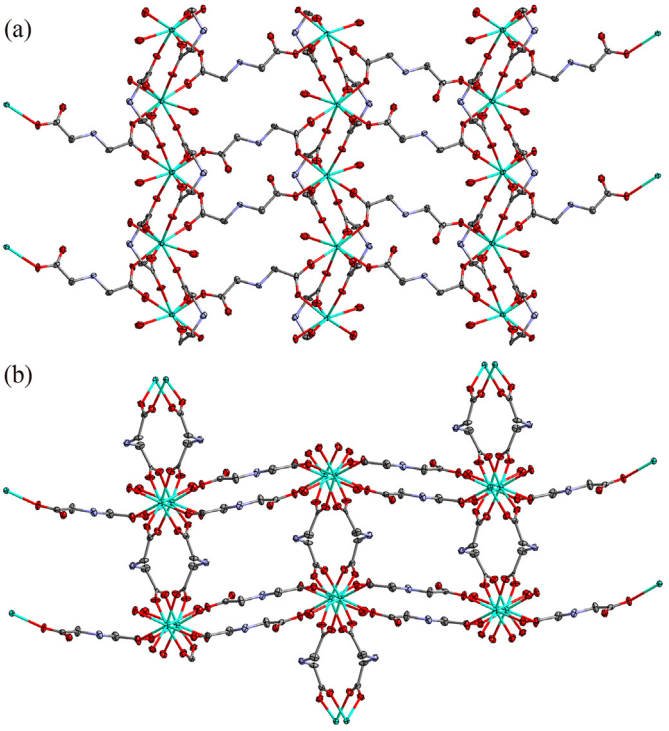

Fig. 3. The extended structures of **3** viewed along the *bc* plane (a) and the *ab* plane (b). H atoms and ClO_4^- ions are omitted for clarity. Color legend: Eu (cyan), O (red), C (grey), and N (purple).

5, viewed along the crystallographic *a*-axis; the structures are similar, but the fine differences are clearly noticeable (Fig. 4).

For the series of lanthanide tartrates (**7**–**10**), all four compounds are isostructural in the tetragonal space group of $P4_12_12$. We note that such a structural type had already been reported[35–37,47–51]; the lanthanide ion is nona-coordinate, displaying a tricapped trigonal prismatic coordination geometry with three aqua ligand O atoms and six tartrate O atoms. The overall framework structure

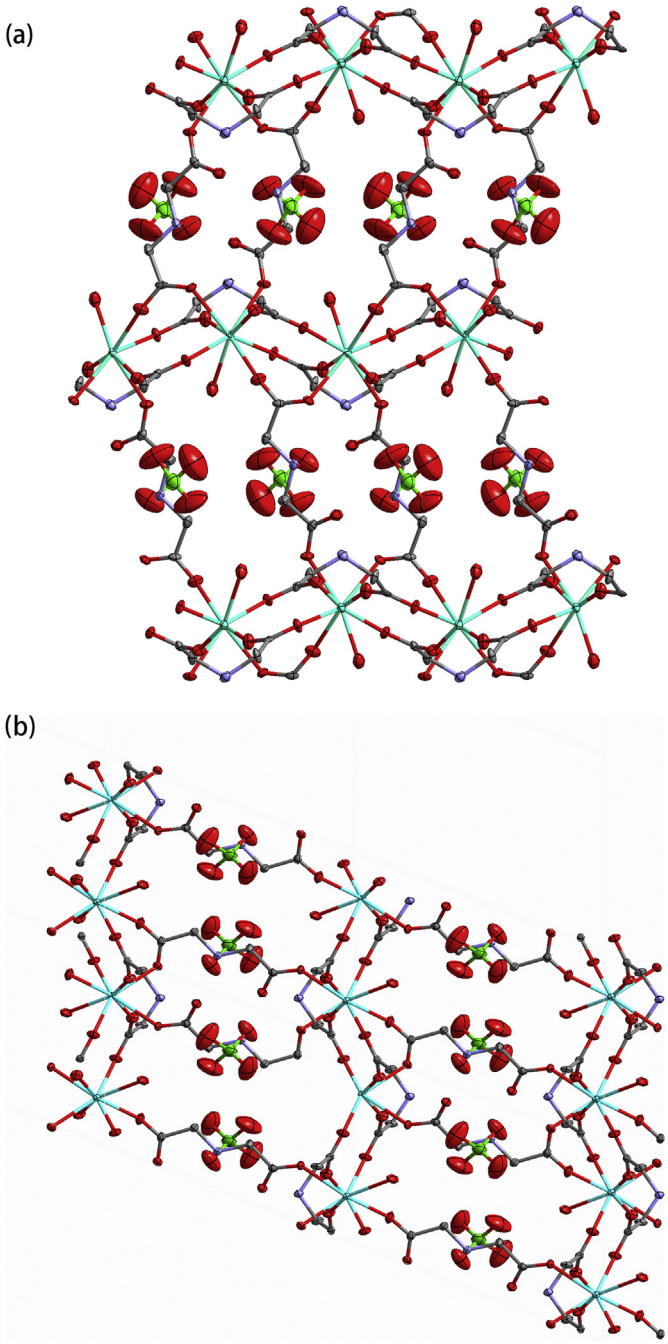

Fig. 4. The structures of **3** (a) and **5** (b) viewed along the *a*-axis.

can be viewed as a 2D chiral sheet of Eu(III)-tartrate hydrogen-bonded by the aqua ligands (Fig. S1). The mixed-lanthanide complexes **11a**–**e** showed the same powder X-ray diffraction patterns as their single-lanthanide cognates (Fig. S2) are therefore isostructural to **7**–**10**.

3.3. Photoluminescence studies

Upon UV irradiation at 365 nm, **3** and **5** displayed intense red and green emissions characteristic of Eu(III) and Tb(III), respectively (Fig. 5). The mixed-lanthanide (Eu/Tb) complex **6** showed yellow emission under the same conditions (Fig. 5, middle).

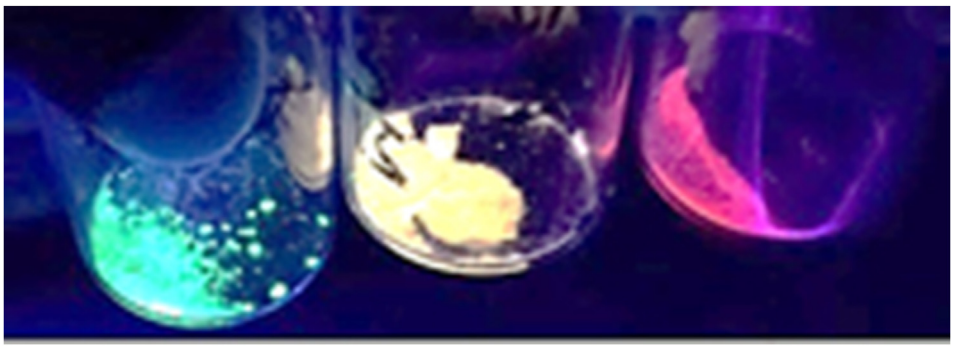

Fig. 5. Luminescence of **3** (right), **5** (left), and **6** (middle) under UV irradiation at 365 nm.

The solid-state excitation and emission spectra of **2**, **3**, **5**, and **6** were measured at room temperature. The time-resolved phosphorescence spectra of the Gd(III) complex **4** were obtained at 77 K (Fig. S4). As the lowest excited state of Gd(III) ($^6P_{7/2}$) is too high to accept energy from the ligand,[52] the data obtained by deconvoluting the phosphorescence spectrum of **4** into its Franck-Condon progression with the highest energy component taken as the 0–0 transition yielded the triplet energy the ligand. This energy, determined to be 25200 cm^{-1}, falls in the right energy range of 22000–27000 cm^{-1} for the sensitization of Eu(III) and Tb(III)-based luminescence. However, as is discussed below, we observe that the excitation spectra show mostly direct f–f excitation bands, indicating that direct excitation is prevalent with a smaller contribution from the T_1 state of the ligand.[4,23] As such, quantum yields of sensitized emission were not determined because the excitation occurs mostly independently of the ligands and the antenna effect is negligible.

Complex **2** displayed metal-centered emission in the near-infrared (NIR) range upon excitation at 461 nm, as is shown by the purple trace in Fig. 6(a). The two sharp bands in the emission spectrum correspond to the $^4F_{3/2} \rightarrow {}^4I_J$ ($J = 11/2, 13/2$) transitions; the former at about 1063 nm is most useful in laser systems and the latter at about 1370 nm more useful for telecommunication applications.[53,54]

Upon excitation at 393.4 nm, **3** displayed Eu(III)-centered emissions (Fig. 6(b)) featuring sharp bands corresponding to the $^5D_0 \rightarrow {}^7F_J$ ($J = 1, 2, 3, 4$) transitions into the ground-state manifold. All emission bands exhibit extensive Stark fine structure, including a very intense $^5D_0 \rightarrow {}^7F_4$ emission, indicative of low symmetry around the Eu(III) center.[32] It is known that the $^5D_0 \rightarrow {}^7F_2$ transition is electric-dipole allowed and hypersensitive to the site symmetry, whereas the $^5D_0 \rightarrow {}^7F_1$ transition is magnetic-dipole allowed and insensitive to the site symmetry. The intensity ratio of the $^5D_0 \rightarrow {}^7F_2$ transition to the $^5D_0 \rightarrow {}^7F_1$ transition therefore reveals important structural information such as the site symmetry of Eu(III) and the ligand environments.[7,18] In the present case, the more intense transition of $^5D_0 \rightarrow {}^7F_2$ suggests that the coordination environment of the Eu(III) is non-centrosymmetric and without an inversion center, which is in good agreement with the structure determined crystallographically. The excitation spectrum, obtained by monitoring the most intense emission band at 612 nm originating from the $^5D_0 \rightarrow {}^7F_2$ transition is dominated by sharp bands, corresponding to excitation into higher metal-centered energy levels. A less intense broad band with a maximum at approximately 260 nm corresponds to a less efficient ligand-centered excitation.

As is shown in Fig. 6(c), **5** showed green emission dominated by the expected sharp emission bands of the $^5D_4 \rightarrow {}^7F_J$ ($J = 6, 5, 4, 3, 2, 1, 0$) transitions into the ground-state manifold of Tb(III). The excitation spectrum, shown as the black trace, was obtained by monitoring the emission of the most intense peak at 544 nm, corresponding to the hypersensitive $^5D_4 \rightarrow {}^7F_5$ transition which is responsible for the intense green luminescence in solid state. This spectrum displays a broad band with a maximum at 266 nm, corresponding to a ligand-based transition; again, the most intense transitions are the sharp bands in the range of 275–390 nm, which correspond to direct excitation into higher metal-centered levels. Each emission band from $^5D_4 \rightarrow {}^7F_6$ to $^5D_4 \rightarrow {}^7F_3$ splits into two peaks, suggesting a strong low-symmetry crystal field in **5**.[22]

The mixed-lanthanide (Eu/Tb) complex **6** has interesting excitation and emission spectra (Fig. 7). When the excitation was monitored at the maximum of Eu(III) emission at 619 nm, an excitation spectrum showing a combination of Eu(III) and Tb(III) transitions was obtained (Fig. 7(a)). On the other hand, when the excitation was monitored at the maximum Tb(III) emission at 544 nm, the excitation spectrum displayed features more closely associated with the excitation of the Tb(III) complex (Fig. 7(a)). This

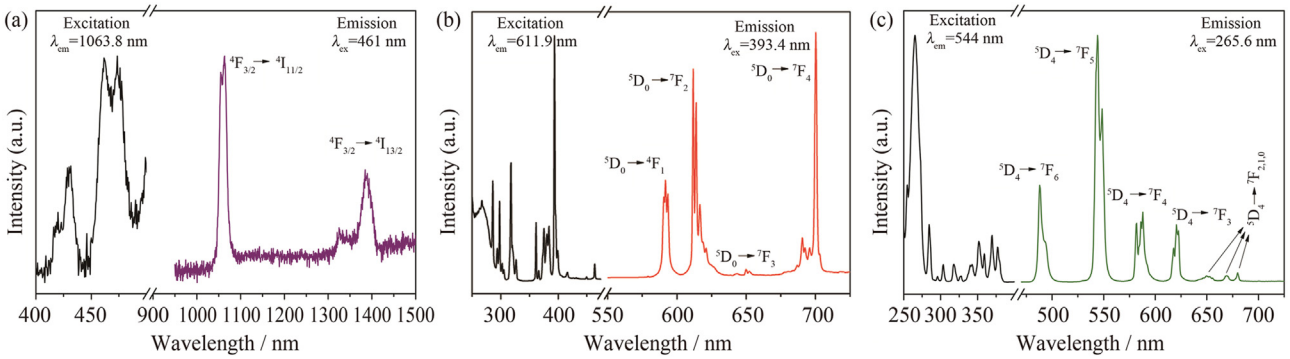

Fig. 6. Solid-state excitation and emission spectra of **2** (a), **3** (b) and **5** (c) at room temperature.

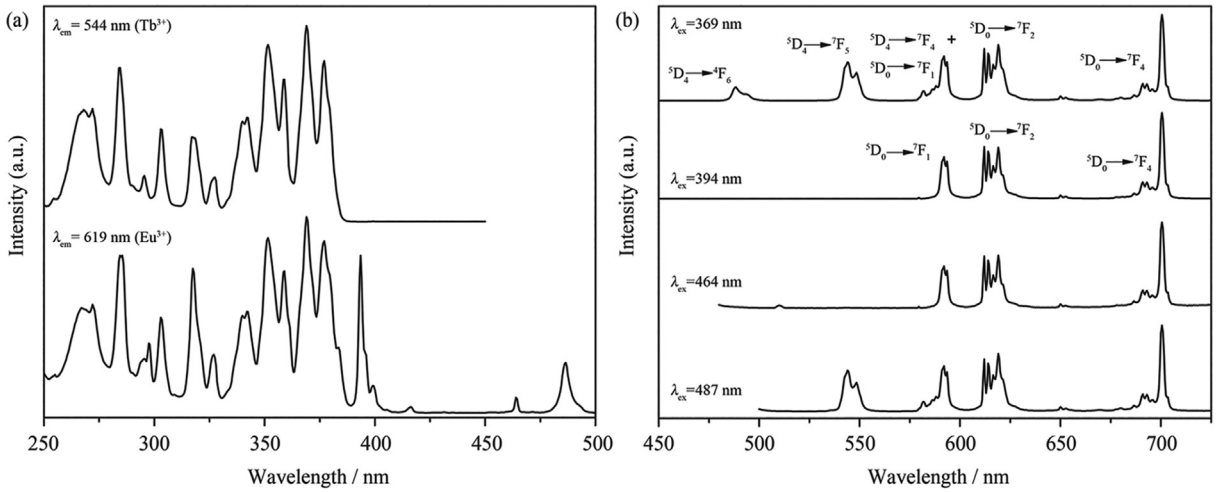

Fig. 7. Excitation (a) and emission (b) spectra of the mixed-lanthanide complex **6**.

is an indication that the pathways for energy transfer go from an f–f excitation into higher-energy levels centered at Tb(III), followed by both Tb(III) emission and energy migration to Eu(III) and subsequent Eu(III)-centered emission. This can be seen upon closer inspection of the emission spectra (Fig. 7(b)) obtained at different excitation wavelengths. The top spectrum, which was obtained with an excitation at 369 nm ($^5L_8 \leftarrow {}^7F_0$ and $^5L_{10} \leftarrow {}^7F_6$ transitions of Eu(III) and Tb(III), respectively), showed emission bands originating from both Eu(III) and Tb(III). As the excitation is shifted to a lower energy at 394 nm ($^5L_6 \leftarrow {}^7F_0$ transition of Eu(III)), the Tb(III)-based bands disappeared and only the Eu(III)-centered emission bands are present. As the excitation wavelength is shifted to even lower energy, the intensity of the Tb(III)-based bands decreases and increasingly Eu(III)-centered emission is seen.

These results can also be appreciated visually as is shown in Fig. 8: Excitation of complex **6** at 369 nm led to a yellow emission (Fig. 8(a)), which is a combination of red and green, while an excitation at 394 nm led to Eu(III)-centered red emission only (Fig. 8(b)).

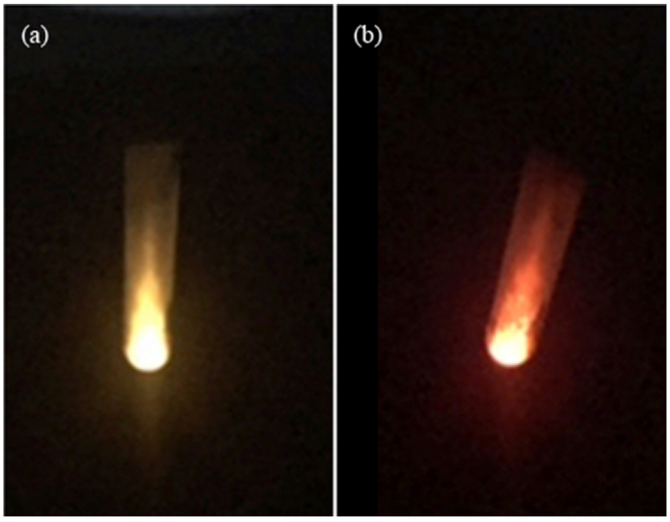

Fig. 8. Emission of complex **6** in the solid state under different excitation wavelengths. (a) $\lambda_{ex} = 369$ nm; (b) $\lambda_{ex} = 394$ nm.

Table 1
Emission lifetimes of the complexes **3**, **5**, and **6** measured in the solid state.

Complexes	Transition	τ (ms)
3, Eu(III)	$^5D_0 \rightarrow {}^7F_2$	0.723 ± 0.009
5, Tb(III)	$^5D_4 \rightarrow {}^7F_5$	1.601 ± 0.058
6, Eu(III)/Tb(III)	$^5D_0 \rightarrow {}^7F_2$	0.866 ± 0.016
($\lambda_{ex} = 369$ nm)	$^5D_4 \rightarrow {}^7F_5$	0.436 ± 0.013

Emission lifetimes of the complexes, typical of any lanthanide complexes, are summarized in Table 1. However, it is interesting to note that the Tb(III)-centered lifetime of the mixed-lanthanide

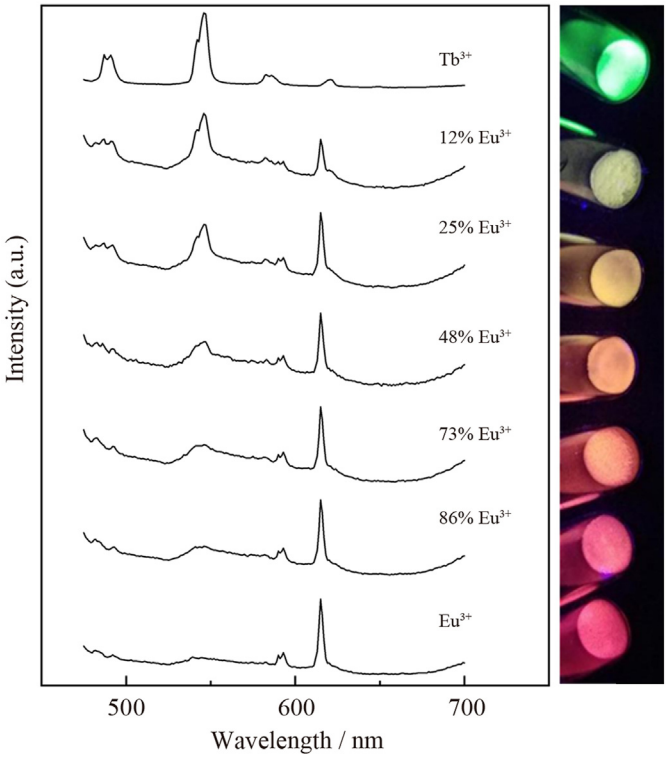

Fig. 9. Emission spectra ($\lambda_{ex} = 365$ nm) of the mixed-lanthanide tartrates with systematically altered Eu(III)/Tb(III) ratio.

complex **6** is shorter than that of **4**, a consequence of the energy transfer from Tb(III) to Eu(III). These results suggest that for the mixed-lanthanide complex, excitation leads to energy transfer from one lanthanide ion to the other, resulting in an enhancement of the luminescence of that other ion instead of stimulating emissions from each ion.[16,21,55] The efficiency of energy transfer η_{ET} is 72.7%, on the same order of magnitude as was reported for other mixed lanthanide systems.[56,57]

Similar to the lanthanide iminodiacetates, the color of emission can also be tuned by changing the ratio of different lanthanide ions in the mixed-lanthanide tartrates. Upon excitation at 365 nm, a series of gradually changing colors of emission between the intense green emission of Tb(III) and the red emission of Eu(III) was observed as the amount of Eu(III) in the reaction mixture increased (Fig. 9). Excitation and emission spectra for **7**, **9**, and **11a**–**e** are shown in Figs. S4-S10. It is interesting to note that only a small amount of Eu(III) was needed for the mixed-lanthanide complex to exhibit the $^5D_0 \rightarrow {}^7F_2$ transition. Again, this observation is consistent with the intra-MOF energy transfer from Tb(III) to Eu(III).[10,13,21–23] By making use of this unique mechanism of energy transfer and the resulting luminescence properties, fluorescent sensors[58–65] and luminescent thermometers[15,66,67] have been developed.

4. Conclusions

Two series of lanthanide-containing complexes with three-dimensional framework structures with iminodiacetate and tartrate as respective ligands were synthesized and structurally characterized. The photophysical properties of these complexes were investigated. It was shown that both systems display red and green luminescence for the Eu(III) and Tb(III) analogs, respectively. Using lanthanide mixtures of Eu(III) and Tb(III), isostructural mixed-lanthanide complexes were also obtained. Transfer of excitation energy from Tb(III) to Eu(III) is evident from the emission spectra of these bimetallic complexes. As such, the color of emission can be tuned by varying the relative amount of the component lanthanide ions. Efforts to produce white light from one single mixed-lanthanide complex containing multiple lanthanide ions are underway.

Acknowledgements

This work was supported in part by US NSF grant CHE-1800392 (AdBD). The authors thank Dr. Chad Park for assistance with the photophysical studies. We also acknowledge the Arizona Laboratory for the use of the ICP-MS supported by NIEHS Grant (P42 ES-04940-11).

Appendix A. Supplementary data

Supplementary data to this article can be found online at https://doi.org/10.1016/j.jre.2021.01.019.

References

1. Luo TY, Das P, White DL, Liu C, Star A, Rosi NL. Luminescence "turn-on" detection of gossypol using Ln^{3+}-based metal-organic frameworks and Ln^{3+} salts. *J Am Chem Soc*. 2020;142:2897.
2. Liu W, Chen CY, Wu ZL, Pan YF, Ye CH, Mu ZR, et al. Construction of multifunctional luminescent lanthanide MOFs by hydrogen bond functionalization for picric acid detection and fluorescent dyes encapsulation. *ACS Sustain Chem Eng*. 2020;8(35):13497.
3. Zhao YF, Li D. Lanthanide-functionalized metal–organic frameworks as ratiometric luminescent sensors. *J Mater Chem C*. 2020;8(37):12739.
4. Mahata P, Mondal SK, Singha DK, Majee P. Luminescent rare-earth-based MOFs as optical sensors. *Dalton Trans*. 2017;46(2):301.
5. Lustig WP, Mukherjee S, Rudd ND, Desai AV, Li J, Ghosh SK. Metal–organic frameworks: functional luminescent and photonic materials for sensing applications. *Chem Soc Rev*. 2017;46(11):3242.
6. Hu Z, Deibert BJ, Li J. Luminescent metal–organic frameworks for chemical sensing and explosive detection. *Chem Soc Rev*. 2014;43(16):5815.
7. Cui YJ, Yue YF, Qian GD, Chen BL. Luminescent functional metal–organic frameworks. *Chem Rev*. 2012;112(2):1126.
8. Zhang QS, Wang J, Kirillov AM, Dou W, Xu C, Xu CL, et al. Multifunctional Ln–MOF luminescent probe for efficient sensing of Fe^{3+}, Ce^{3+}, and acetone. *ACS Appl Mater Inter*. 2018;10(28):23976.
9. Wang FQ, Pu YQ, Zhang XM, Zhang FX, Cheng HG, Zhao YN. A series of multifunctional lanthanide metal-organic frameworks for luminescent sensing and photocatalytic applications. *J Lumin*. 2019;206:192.
10. Yan B. Lanthanide-functionalized metal–organic framework hybrid systems to create multiple luminescent centers for chemical sensing. *Acc Chem Res*. 2017;50(11):2789.
11. Gu DX, Yang WT, Lin DY, Qin XD, Yang YH, Wang FX, et al. Water-stable lanthanide-based metal–organic gel for the detection of organic amines and white-light emission. *J Mater Chem C*. 2020;8(39):13648.
12. Xu LN, Li YN, Pan QJ, Wang D, Li SJ, Wang GF, et al. Dual-mode light-emitting lanthanide metal–organic frameworks with high water and thermal stability and their application in white LEDs. *ACS Appl Mater Inter*. 2020;12(16):18934.
13. Liu ZF, Wu MF, Wang SH, Zheng FK, Wang GE, Chen J, et al. Eu^{3+}-doped Tb^{3+} metal–organic frameworks emitting tunable three primary colors towards white light. *J Mater Chem C*. 2013;1(31):4634.
14. Wu YP, Xu GW, Dong WW, Zhao J, Li DS, Zhang J, et al. Anionic lanthanide MOFs as a platform for iron-selective sensing, systematic color tuning, and efficient nanoparticle catalysis. *Inorg Chem*. 2017;6(3):1402.
15. An R, Zhao H, Hu HM, Wang X, Yang ML, Xue G. Synthesis, structure, white-light emission, and temperature recognition properties of Eu/Tb mixed coordination polymers. *Inorg Chem*. 2016;55(2):871.
16. Ma ML, Ji C, Zang SQ. Syntheses, structures, tunable emission and white light emitting Eu^{3+} and Tb^{3+} doped lanthanide metal–organic framework materials. *Dalton Trans*. 2013;42(29):10579.
17. Rao XT, Huang Q, Yang XL, Cui YJ, Yang Y, Wu CD, et al. Color tunable and white light emitting Tb^{3+} and Eu^{3+} doped lanthanide metal–organic framework materials. *J Mater Chem*. 2012;22(7):3210.
18. Cui YJ, Chen BL, Qian GD. Lanthanide metal-organic frameworks for luminescent sensing and light-emitting applications. *Coord Chem Rev*. 2014;273–274:76.
19. Karmakar A, Samanta P, Desai AV, Ghosh SK. Guest-responsive metal–organic frameworks as scaffolds for separation and sensing applications. *Acc Chem Res*. 2017;50(10):2457.
20. Mi XN, Sheng DF, Yu Y, Wang YH, Zhao LM, Lu J, et al. Tunable light emission and multiresponsive luminescent sensitivities in aqueous solutions of two series of lanthanide metal–organic frameworks based on structurally related ligands. *ACS Appl Mater Inter*. 2019;11(8):7914.
21. Tang Q, Liu SX, Liu YW, He DF, Miao J, Wang XQ, et al. Color tuning and white light emission via *in situ* doping of luminescent lanthanide metal–organic frameworks. *Inorg Chem*. 2014;53(1):289.
22. da Luz LL, Lucena Viana BF, da Silva GCO, Gatto CC, Fontes AM, Malta M, et al. Controlling the energy transfer in lanthanide–organic frameworks for the production of white-light emitting materials. *CrystEngComm*. 2014;16(30):6914.
23. Wu JW, Zhang HB, Du SW. Tunable luminescence and white light emission of mixed lanthanide–organic frameworks based on polycarboxylate ligands. *J Mater Chem C*. 2016;4(16):3364.
24. Bünzli JCG. Benefiting from the unique properties of lanthanide ions. *Acc Chem Res*. 2006;39(1):53.
25. Bünzli JCG, Comby S, Chauvin AS, Vandevyver CDB. New opportunities for lanthanide luminescence. *J Rare Earths*. 2007;25(3):257.
26. Seitz M, Oliver AG, Raymond KN. The lanthanide contraction revisited. *J Am Chem Soc*. 2007;129(36):11153.
27. de Bettencourt-Dias A. New isophthalato-based 2D coordination polymers of Eu(III), Gd(III) and Tb(III) - enhancement of the terbium-centered luminescence through thiophene derivatization. *Inorg Chem*. 2005;44:2734.
28. Zhao D, Rao XT, Yu JC, Cui YJ, Yang Y, Qian GD. Design and synthesis of an MOF thermometer with high sensitivity in the physiological temperature range. *Inorg Chem*. 2015;54(23):11193.
29. Abdelhamid HN, Wilk-Kozubek M, El-Zohry AM, Bermejo Gómez A, Valiente A, Martín-Matute B, et al. Luminescence properties of a family of lanthanide metal-organic frameworks. *Micropor Mesopor Mater*. 2019;279:400.
30. Albertsson J, Oskarsson Å, Glehn M, Tolboe O, Paasivirta J. On the crystal structure of the neodymium iminodiacetate compound $Nd_2(C_4H_5O_4N)_3 \cdot 2HCl \cdot 7H_2O$. *Acta Chem Scand*. 1968;22:1700.
31. Albertsson J, Oskarsson Å. Structural studies on the rare earth carboxylates. 23. The crystal structure of tetra-aquobis(hydrogeniminodiacetato)-iminodiacetatodipraseodymium(3+) dichloride trihydrate at -50 degrees C. *Acta Chem Scand*. 1974;A28:347.
32. Zhang LM, Deng DY, Peng G, Sun L, Liang L, Lan GQ, et al. A series of three-dimensional (3D) chiral lanthanide coordination polymers generated by spontaneous resolution. *CrystEngComm*. 2012;14(23):8083.
33. Kremer C, Morales P, Torres J, Castiglioni J, González-Platas J, et al. Novel lanthanide–iminodiacetate frameworks with hexagonal pores. *Inorg Chem Commun*. 2008;11(8):862.

34. Zhang LM, Yu NQ, Zhang KH, Qiu RS, Zhao YX, Rong WC, et al. Syntheses, structure, and properties of a series of three-dimensional lanthanide-based hybrid frameworks. *Inorg Chim Acta*. 2013;400:67.
35. Hawthorne FC, Borys I, Ferguson RB. Structure of erbium ditartrate trihydrate, $Er^{4+}\cdot 2C_4H_4O_6^{2-}\cdot 3H_2O$. *Acta Crystallogr C: Struct Chem*. 1983;39(5):540.
36. Wu CD, Zhan XP, Lu CZ, Zhuang HH, Huang JS. Poly[triaqua([mu]-hydrogen tartrato)([mu]-tartrato)samarium(III)]. *Acta Crystallogr E: Crystallogr Commun*. 2002;58(5):m228.
37. Yan PF, Xing JC, Li GM, Sun WB, Zhang JW, Hou GF. Two- and three-dimensional coordination polymers of lanthanide tartrate: synthesis, crystal structures and luminescence. *J Coord Chem*. 2009;62(13):2095.
38. Sheldrick GM. *Shelxl*. University of Gottingen; 2014.
39. Spek AL. Structure validation in chemical crystallography. *Acta Crystallogr D*. 2009;65(2):148.
40. Crosby GA, Whan RE, Alire RM. Intramolecular energy transfer in rare earth chelates. Role of the triplet state. *J Chem Phys*. 1961;34(3):743.
41. Cai YP, Li GB, Zhan QG, Sun F, Zhang JG, Gao S, et al. Syntheses and characterization of the samarium(III)–copper(II) 3D coordination network constructed by iminodiacetic acid. *J Solid State Chem*. 2005;178(12):3729.
42. Ren YP, Long LS, Mao BW, Yuan YZ, Huang RB, Zheng LS. Nanoporous lanthanide–copper(II) coordination polymers: syntheses and crystal structures of $[\{M_2(Cu_3(iminodiacetate)_6)\}\cdot 8H_2O]_n$ (M=La, Nd, Eu). *Angew Chem Int Ed*. 2003;42(5):532.
43. Xu HB, Zhao YH, Su ZM, Li GH, Ma Y, Shao KZ, et al. Syntheses and structure of a novel layered lanthanide–zinc coordination polymer: $[LaZn(HIDA)(IDA)_2\cdot 0.5H_2O]_n$. *Chem Lett*. 2004;33(4):446.
44. Xu W, Zhang CJ, Wang H, Wang Y. Two novel two-dimensional lanthanide (III) coordination polymers constructed from isonicotinic acid and iminodiacetic acid: synthesis, structure, and luminescence properties. *J Clust Sci*. 2017;28(4):2005.
45. Dong HL, Xu L. The first lanthanide(III)–iminodiacetate coordination polymer. *Inorg Chem Commun*. 2006;9(4):379.
46. Viswanathan S, de Bettencourt-Dias A. 2-Chloro-5-nitrobenzoato complexes of Eu(III) and Tb(III) – a 1D coordination polymer and enhanced solution luminescence. *Inorg Chem Commun*. 2006;9(5):444.
47. Want B, Ahmad F, Kotru PN. Dielectric and thermal behaviour of holmium tartrate trihydrate crystals. *Cryst Res Technol*. 2007;42(8):822.
48. Want B, Ahmad F, Kotru PN. Growth of ytterbium tartrate trihydrate crystals in silica and agar-agar gels and their characterization. *Cryst Res Technol*. 2006;41(12):1167.
49. Want B, Ahmad F, Kotru PN. Crystal growth and characterization of gadolinium tartrate trihydrate: $Gd(C_4H_4O_6)(C_4H_5O_6)\cdot 3H_2O$. *Mater Sci Eng A*. 2006;431(1):237.
50. Almond MJ, Drew MGB, Morris S, Rice DA. A single crystal X-ray diffraction study of yttrium tartrate hydrate $[Y(C_4H_4O_6)(C_6H_5O_6)\cdot 2.5H_2O]$. *Polyhedron*. 1996;15(19):3377.
51. Xu W, Chang HS, Liu W, Zheng YQ. Synthesis, crystal structure, and properties of a new lanthanide tartrate coordination polymer. *Russ J Coord Chem*. 2014;40(4):251.
52. Wang YW, Zhang YL, Dou W, Zhang AJ, Qin WW, Liu WS. Synthesis, radii dependent self-assembly crystal structures and luminescent properties of rare earth (III) complexes with a tripodal salicylic derivative. *Dalton Trans*. 2010;39(38):9013.
53. Comby S, Bünzli JCG. Lanthanide near-infrared luminescence in molecular probes and devices. In: Gschneidner Jr KA, Bünzli JCG, Pecharsky VK, eds. *Handbook on the Physics and Chemistry of Rare Earths*. vol. 37. Amsterdam: Elsevier; 2007:217.
54. George TM, Varughese S, Reddy MLP. Near-infrared luminescence of Nd^{3+} and Yb^{3+} complexes using a polyfluorinated pyrene-based β-diketonate ligand. *RSC Adv*. 2016;6(73):69509.
55. Liu K, You HP, Zheng YH, Jia G, Song YH, Huang YJ, et al. Facile and rapid fabrication of metal–organic framework nanobelts and color-tunable photoluminescence properties. *J Mater Chem*. 2010;20(16):3272.
56. Bao G, Wong KL, Jin D, Tanner PA. A stoichiometric terbium-europium dyad molecular thermometer: energy transfer properties. *Light Sci Appl*. 2018;7(1):96.
57. Xia M, Wu XB, Zhong Y, Hintzen HT, Zhou Z, Wang J. Photoluminescence properties and energy transfer in a novel $Sr_8ZnY(PO_4)_7$:Tb^{3+}, Eu^{3+} phosphor with high thermal stability and its great potential for application in warm white light emitting diodes. *J Mater Chem C*. 2019;7(10):2927.
58. Zhang YH, Li B, Ma HP, Zhang LM, Zheng YX. Rapid and facile ratiometric detection of an anthrax biomarker by regulating energy transfer process in bio-metal-organic framework. *Biosens Bioelectron*. 2016;85:287.
59. Zhang YH, Li B, Ma HP, Zhang LM, Jiang H, Song H, et al. A nanoscaled lanthanide metal–organic framework as a colorimetric fluorescence sensor for dipicolinic acid based on modulating energy transfer. *J Mater Chem C*. 2016;4(30):7294.
60. Shen ML, Liu B, Xu L, Jiao H. Ratiometric fluorescence detection of anthrax biomarker 2, 6-dipicolinic acid using hetero MOF sensors through ligand regulation. *J Mater Chem C*. 2020;8(13):4392.
61. Yilmaz MD, Oktem HA. Eriochrome black Tb^{3+}–Eu^{3+} complex as a ratiometric colorimetric and fluorescent probe for the detection of dipicolinic acid, a biomarker of bacterial spores. *Anal Chem*. 2018;90(6):4221.
62. Othong J, Boonmak J, Kielar F, Hadsadee S, Jungsuttiwong S, Youngme S. Self-calibrating sensor with logic gate operation for anthrax biomarker based on nanoscaled bimetallic lanthanoid MOF. *Sens Actuators B*. 2020:128156.
63. Wu MN, Zhuang YX, Liu JB, Chen WW, Li XY, Xie RJ. Ratiometric fluorescence detection of 2, 6-pyridine dicarboxylic acid with a dual-emitting lanthanide metal-organic framework (MOF). *Opt Mater*. 2020;106, 110006.
64. Chen XB, Qi CX, Xu YB, Li H, Xu L, Liu B. A quantitative ratiometric fluorescent Hddb-based MOF sensor and its on-site detection of the anthrax biomarker 2, 6-dipicolinic acid. *J Mater Chem C*. 2020;8(48):17325.
65. Lei H, Qi CX, Chen XB, Zhang T, Xu L, Liu B. Ratiometric fluorescence determination of the anthrax biomarker 2, 6-dipicolinic acid using a Eu^{3+}/Tb^{3+}-doped nickel coordination polymer. *New J Chem*. 2019;43(46):18259.
66. Cui YJ, Xu H, Yue YF, Guo ZY, Yu JC, , et alChen BL. A luminescent mixed-lanthanide metal–organic framework thermometer. *J Am Chem Soc*. 2012;134(9):3979.
67. Yang Y, Chen L, Jiang FL, Yu MX, Wan XY, , et alHong MC. A family of doped lanthanide metal–organic frameworks for wide-range temperature sensing and tunable white light emission. *J Mater Chem C*. 2017;5(8):1981.